

Skyrmionic state and stable half-quantum vortices in chiral p -wave superconductors

Julien Garaud^{1,2} and Egor Babaev^{1,2}

¹*Department of Physics, University of Massachusetts Amherst, MA 01003 USA*

²*Department of Theoretical Physics, The Royal Institute of Technology, Stockholm, SE-10691 Sweden*

Observability of half-quantum vortices and skyrmions in p -wave superconductors is an outstanding open question. Under the most common conditions, fractional flux vortices are not thermodynamically stable in bulk samples. Here we show that in chiral p -wave superconductors, there is a regime where, in contrast lattices of integer flux vortices are not thermodynamically stable. Instead skyrmions made of spatially separated half-quantum vortices are the topological defects produced by an applied external field.

PACS numbers: 74.20.Rp, 74.25.Dw, 74.25.Ha

Higher broken symmetries in p -wave superconductors have inspired long-standing interest to realize topological defects more complicated than vortices. Much of the early discussions of various complex topological defects were in the context of superfluid ^3He .¹ Recently attention to these questions has raised dramatically in connection with superconductors which are argued to have p -wave pairing, such as Sr_2RuO_4 . The highly interesting possibility there, is connected with half-quantum vortices.²⁻⁸ Their statistics is non-Abelian and they could potentially be used for quantum computations.⁹ Other kinds of topological defects discussed in connection with spin-triplet superconductors are skyrmions¹⁰ and hopfions.¹¹ In superconducting materials, the creation of these topological excitations is highly nontrivial. Superconducting components are coupled by a gauge field and there are also symmetry-reducing inter-component interactions. As a consequence fractional vortices have logarithmically or linearly divergent energies (see *e.g.* Ref. 8), while integer flux vortices have finite energy per unit length. Consequently, under usual conditions, half-quantum vortices are thermodynamically unstable in bulk systems. It was argued that complex setups, such as mesoscopic samples, are needed for their creation.^{2,8,12} Recently it was claimed that a half-quantum vortex was observed in a mesoscopic sample of Sr_2RuO_4 .² Other proposed routes to observe fractional vortices, invoke (i) thermal deconfinement,^{3,6,13} (ii) potential materials with strongly reduced spin stiffness⁴ and (iii) regimes very close to the upper critical magnetic field, where gauge-field mediated half-quantum vortex confinement is weak.⁵ In some more general systems it was shown that fractional vortices could be thermodynamically stable near boundaries.¹⁴ Today the conditions under which half-quantum vortices and skyrmions¹⁰ could be experimentally created in bulk superconductors still remains an outstanding open question.

In this work we investigate the magnetic response of the Ginzburg-Landau model the has been widely applied to Sr_2RuO_4 .^{15,16} Our considerations apply to two-dimensional systems or three-dimensional problems with translation invariance along the z -direction. Then the free energy density reads

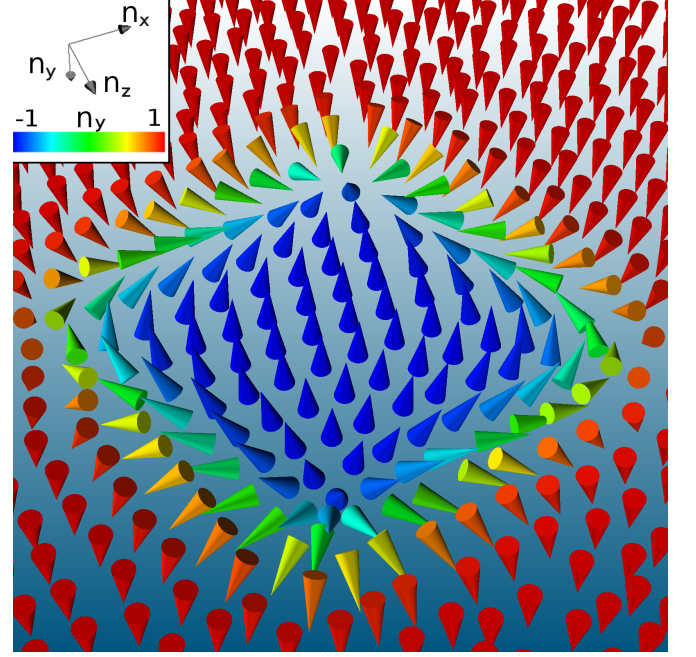


Figure 1. (Color on-line) – Numerically calculated texture of the pseudo-spin vector for a skyrmion carrying with a topological charge $Q = 2$. As can be seen in the picture the skyrmionic topological charge density is confined in a closed domain wall.

$$\mathcal{F}(\psi_a, \mathbf{A}) = |\nabla \times \mathbf{A}|^2 \quad (1a)$$

$$+ |D_x \psi_1|^2 + |D_y \psi_2|^2 + \gamma |D_y \psi_1|^2 + \gamma |D_x \psi_2|^2 + 2\gamma \text{Re}[(D_x \psi_1)^* D_y \psi_2 + (D_y \psi_1)^* D_x \psi_2] \quad (1b)$$

$$+ (2\gamma - 1)|\psi_1|^2 |\psi_2|^2 + \sum_{a=1,2} -|\psi_a|^2 + \frac{1}{2}|\psi_a|^4 \quad (1c)$$

$$+ \gamma |\psi_1|^2 |\psi_2|^2 \cos(2(\varphi_2 - \varphi_1)). \quad (1d)$$

The different components of the order parameter are denoted $\psi_{1,2} = |\psi_{1,2}|e^{i\varphi_{1,2}}$; $\mathbf{D} = \nabla + ie\mathbf{A}$. The p -wave state is described here by a doublet of complex fields subjected to the the following symmetry breaking coupling : $\text{Re}(\psi_1^* \psi_2^2) = |\psi_1|^2 |\psi_2|^2 \cos(2(\varphi_2 - \varphi_1))$. The ground state breaks the $U(1) \times \mathbb{Z}_2$ symmetry, since the ground state phase difference is either $\pi/2$ or $3\pi/2$. Gradient

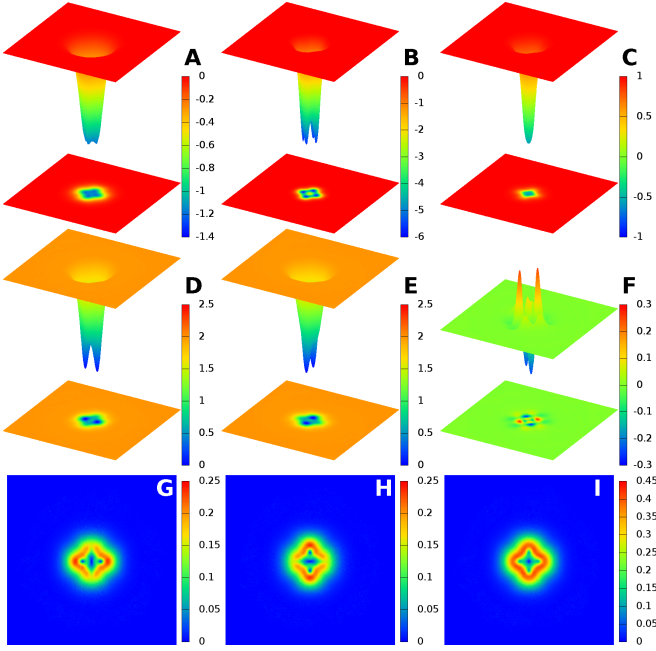


Figure 2. (Color on-line) – A thermodynamically stable skyrmion carrying two flux quanta, with $e = 0.8$ and $\gamma = 0.5$. Displayed quantities are, magnetic flux (A), the (inverted) energy density (B) and the sine of the phase difference $\sin(\varphi_2 - \varphi_1)$ (C). On the second line, the densities of superconducting order parameter components $|\psi_1|^2$ (D), $|\psi_2|^2$ (E), and the ‘doubled phase difference’ $\text{Im}(\psi_1^* \psi_2^2)$ (F). Panels (G) and (resp. H) on the third line are the supercurrents associated with each component ψ_1 (resp. ψ_2) of the order parameter (see Appendix A for definition). The last panel (I) shows the total supercurrent.

terms (1b) make this model clearly anisotropic in the xy -plane. The coefficient γ , controlling the anisotropy, should be $\gamma > 1/3$ for Sr_2RuO_4 , according to.¹⁵ The coupling constant e is a convenient quantity to parametrize the penetration depth of the magnetic field. The discrete \mathbb{Z}_2 symmetry dictates that the system allows domain wall solutions interpolating between two regions with different phase-locking. Such domain walls are energetically expensive and thus not intrinsically stable. It was suggested that they could be observable if pinned by crystalline defects.¹⁷ Also domain walls formed as dynamic excitations inside vortex lattices were studied extensively in.¹⁸ They could be experimentally observable in these setups since they pin half-quantum vortices.^{17,18}

Returning to the discussion of vortices one can observe that the system (1) has $U(1) \times \mathbb{Z}_2$ broken symmetry. Thus a single half-quantum vortex (with winding only in one of the phases) has linearly diverging energy and thus is not thermodynamically stable.⁸ Also from this broken symmetry, the existence of skyrmionic excitations would not follow. The previous works required higher broken symmetry for the existence of skyrmions.¹⁰ However we show below that there is a considerable window of parameters where the system (1) possesses what

we term as a “skyrmionic phase”. In that phase, mostly because of favorable competition between field gradients and potential and magnetic energies, the system does have *thermodynamically stable* skyrmions while ordinary integer flux vortex lattices are *not* thermodynamically stable. These skyrmions are bound states of spatially separated half-quantum vortices, connected by domain walls. Half-quantum vortices are linearly confined into integer vortices in a bulk sample because of the terms $|\psi_1|^2 |\psi_2|^2 \cos(2(\varphi_2 - \varphi_1))$. However on a (closed) domain wall, a composite vortex should split along this wall, since the above-mentioned term has there, unfavorable values of the phase difference. Indeed, such deconfining allows to reduce energetically unfavorable values of the phase differences. Because of this vortex splitting and resulting repulsive interactions, vortices trapped on domain wall can prevent the collapse of a closed domain wall. The main result of this paper is that we show that these objects are characterized by an integer-valued skyrmionic topological charge and that they can be energetically cheaper than vortices. Such a skyrmion is displayed in Fig. 1, as a texture of a pseudo-spin vector field defined later on.

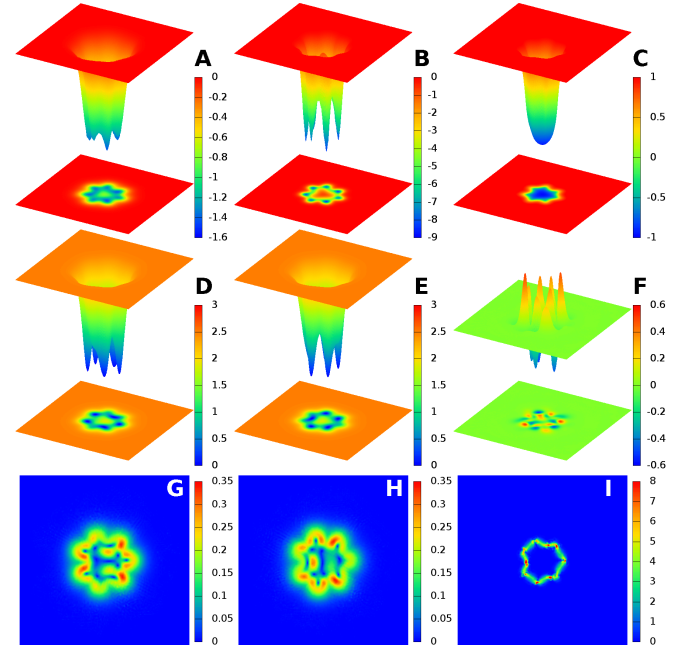


Figure 3. (Color on-line) – A skyrmion carrying five flux quanta, with $e = 0.8$ and $\gamma = 0.4$. Displayed quantities are the same as in Fig. 2, except panel (I) showing the gradient of the phase difference $\nabla\varphi_{12}$, which is non zero at the domain wall. The skyrmion consists of ten spatially separated half-quantum vortices. It assumes a complicated non-symmetric structure due to a competition of a preferred geometry of a skyrmion with the anisotropies (1b).

We investigated structures carrying N flux quanta (*i.e.* with each phase winding $\oint \nabla\varphi_a = 2\pi N$) as functions of the gauge coupling e and the anisotropy parameter γ . Ground states, carrying a given number of magnetic flux

quanta, are computed numerically by minimizing the energy within a finite element framework provided by the Freefem++ library.¹⁹ See technical details in Appendix B.

We find that if the penetration length is sufficiently large (*i.e.* at small values of the coupling constant e), the system indeed forms ordinary Abrikosov vortices in external field. On the other hand for sufficiently large e the system behaves as a type-I superconductor. However there is a regime in a wide range of intermediate coupling constants e , where integer flux vortices are more expensive than bound states of spatially separated half-quantum vortices connected by closed domain wall. Such configurations carrying different number of flux quanta are given in Figures 2, 3 and 4. The clearly visible preferred directions for supercurrents originate in the anisotropies (1b). The cores in different components do not coincide in space. This means fractionalization of vortices in this state. Each of the split cores carries a half of a flux quantum (for detailed calculations of fractional vortices flux quantization, see *e.g.* Ref. 8).

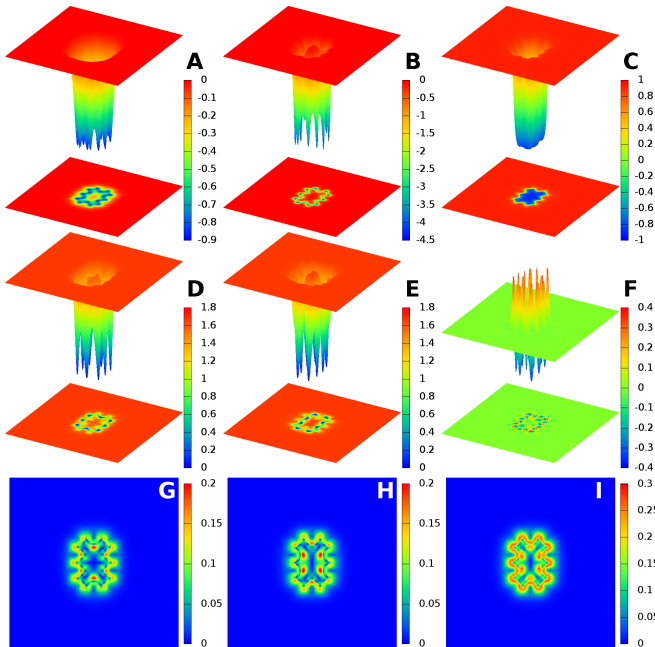


Figure 4. (Color on-line) – A skyrmion with $N = 8$, $e = 0.6$ and in the case of higher anisotropy $\gamma = 0.6$. Displayed quantities are the same as in Fig. 2.

The configurations found here are actually skyrmions, although it may not be obvious from the Figures 2, 3 and 4. To prove that the solutions are skyrmions the two-component model (1) is mapped to an anisotropic non-linear σ -model.²⁰ In that mapping the superconducting condensates are projected on the Pauli matrices σ allowing to define the pseudo-spin vector \mathbf{n} :

$$\mathbf{n} \equiv (n_x, n_y, n_z) = \frac{\Psi^\dagger \boldsymbol{\sigma} \Psi}{\Psi^\dagger \Psi} \quad \text{where} \quad \Psi^\dagger = (\psi_1^*, \psi_2^*). \quad (2)$$

The target space being a sphere, together with the one-point compactification of the plane defines the map $\mathbf{n} : S^2 \rightarrow S^2$. Such maps are classified by the homotopy class $\pi_2(S^2) \in \mathbb{Z}$, so there exists an integer valued topological charge

$$Q(\mathbf{n}) = \frac{1}{4\pi} \int_{\mathbb{R}^2} \mathbf{n} \cdot \partial_x \mathbf{n} \times \partial_y \mathbf{n} \, dx dy. \quad (3)$$

For a skyrmion, $Q = N$, while $Q = 0$ for ordinary vortices. The terms in (1c) and (1d), break the $O(3)$ symmetry of the pseudo-spin \mathbf{n} down to \mathbb{Z}_2 . In a non-linear σ -model, such anisotropy would undermine stability of the skyrmions. However this collapse does not occur in the Ginzburg-Landau model, because of the behaviour of the gradient energy, which is demonstrated below.

The numerically computed topological charge (3) is found to be an integer (with a negligible relative error of the order 10^{-5} , due to the discretization) for the closed domain wall/vortex systems which are therefore skyrmions. The solutions shown in Figures 2, 3 and 4 have skyrmionic topological charge $Q = 2$, $Q = 5$, $Q = 8$ correspondingly. The terminology skyrmion is more intuitively obvious when the solutions are represented in terms of the pseudo-spin vector field \mathbf{n} , as in Fig. 1. However unlike skyrmions in non-linear σ -model, here the skyrmionic topological charge density is mostly concentrated on the half-quantum vortices and on the domain wall.

The main result of this work is that skyrmions of the above type (and thus half-quantum vortices) can be *less energetic* than integer-flux ordinary vortices and *thermodynamically stable*, in the chiral p -wave superconductors. The critical external magnetic field H_{c1} for the formation of a flux-carrying topological defect is determined by the condition where the Gibbs free energy $G = E_d - 2 \int \mathbf{B} \cdot \mathbf{H}_e \, dx dy$ becomes negative. Here E_d and \mathbf{B} are the energy and magnetic field of the defect. \mathbf{H}_e denotes the applied field. Thus $H_{c1} = E_d/2\Phi$ where Φ is the magnetic flux produced by the defect. The defects are thermodynamically stable if the critical external magnetic field's energy density H_{c1}^2 is smaller than the condensation energy. We investigated the energy dependence of the skyrmions on the number of enclosed flux quanta N . The energy of an integer flux vortex is used as a reference point. As shown in Fig. 5 panels (a) and (b), for low N , the energy depends non-monotonically on N . This is because the preferred symmetry of small N configurations in some cases is in strong conflict with the anisotropies of the model. In the large- N limit the energy per flux quantum gradually tends to some value. The main point here is that the energy per flux quantum for skyrmions is in certain cases smaller than that of vortices. This signals instability of vortex lattices with respect to skyrmion formation.

Next, the thermodynamical stability of skyrmions is investigated. Results for $N = 5$ quanta are reported as a characteristic example, in Fig. 5 (c). We find that there are three regimes on the resulting phase diagram.

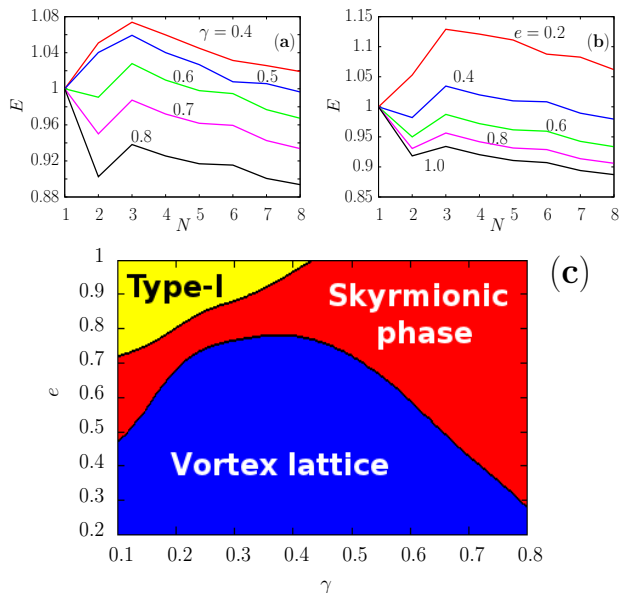


Figure 5. (Color on-line) – Upper panels show the dependence of the energy per flux quantum for skyrmions of different topological charges Q (values are given in the units of the energy of one integer flux vortex). The $N = 1$ point at the origin corresponds to an ordinary vortex solution. Panel (a) shows calculations corresponding to different γ for fixed $e = 0.6$, while (b) displays how the energy per flux quantum changes with e and N for fixed anisotropy parameter $\gamma = 0.7$. The $Q = 2$ skyrmions are usually less energetically expensive than the $Q = 3$. This is because the $Q = 2$ skyrmions can be better aligned with the underlying anisotropies, than the $Q = 3$ skyrmions.

The lower panel displays the *phase diagram*, calculated using energy characteristics of $Q = 5$ skyrmions. The different colors refer to different physical properties. The type-I region is shown by yellow shade. The lower part of the phase diagram shows regions where skyrmions (red) or vortex lattices (blue) form in applied external field. The phase diagram retains similar structure in calculations with different topological charges. With the increasing of the skyrmionic charge Q , the region where skyrmions are energetically preferred over vortex lattices grows slightly. These results apply either for two-dimensional systems or three dimensional systems with translational invariance along z -axis. In the latter case the energy should be understood as the energy per unit length of a skyrmion line (i.e. a skyrmion texture in xy plane which is invariant under translation along z -axis). The discretization errors can be estimated by computing the total magnetic flux and comparing it to the exact value which follows from the quantization condition $2\pi N/e$. This gives the relative accuracy on the flux to be around 10^{-5} . From that, the accuracy on the energy is estimated to be at least three order of magnitude smaller than the energy difference between skyrmions and vortices.

When the penetration length is large (*i.e.* low e), the system shows usual the type-II superconductivity. When the penetration length is small, the system is a type-I superconductor. For intermediate values of the penetration length, depending on the underlying anisotropies γ ,

	E_{total}	E_{grad}	E_{pot}	$E_{\mathbb{Z}_2}$	E_{mag}
Vortex	19.7759	10.7518	-12.0190	16.5195	4.5235
Skyrm.	18.9004	8.10522	-12.2301	17.6336	5.3916
Vortex	32.1684	19.3227	-19.0381	25.4445	6.4392
Skyrm.	37.6456	16.2529	-22.1474	32.8582	10.6818

Table I. Different contributions to the skyrmion energy *per flux quantum*. $Q = 5$ skyrmions are considered in this example. The results are compared with the contributions to the energy of a single vortex (which determines the lower bound on vortex lattice energy near the first critical magnetic field H_{c1}). The gradient contribution E_{grad} is given by the integrated (1b), the magnetic energy E_{mag} by (1a). The potential energy E_{pot} is (1c) and $E_{\mathbb{Z}_2}$ is (1d). First block, for which $\gamma = 0.8$ and $e = 0.4$, corresponds to the state where skyrmions are thermodynamically stable but vortex lattices are not. Second block is for $\gamma = 0.6$ and $e = 0.2$. It corresponds to a regime with standard Abrikosov vortex lattice. Here the skyrmions are local minima of the free energy functional. They are more expensive than vortices but, if formed, they are protected against decay by a finite energy barrier. In the second example the win in the kinetic energy is too small to overcome extra energy cost associated with domain wall formation and magnetic energy.

the external field produces skyrmions rather than vortex lattices. To understand the instability of vortex lattices with respect to skyrmion formation, different contributions to energy are investigated in Table I. In the skyrmionic state, vortex lattice decay into skyrmions is driven by a win in gradient and potential energies although there is a loss in magnetic energy as well as the extra cost of producing a domain wall.

The skyrmions we find are structurally different from skyrmions discussed in other kinds of superconductors¹⁰ because of the different symmetry of the model. Another principal difference is the nature of the skyrmionic state, namely Ref. 10 proposed models where there are only skyrmionic solutions carrying two flux quanta. The latter forming stable lattices. In contrast, the model we consider supports skyrmions with any integer value of topological charge. Importantly, the energy per flux quantum here is a sublinear function of the topological charge, which prohibits a ground state in the form of a lattice of the simplest skyrmions envisaged in Ref. 10. Instead our model predicts more complicated high-topological-charge skyrmionic structures. Also in type-II regime our model predicts metastable states of coexisting vortices and skyrmions.

In conclusion we have shown that the phase diagram of chiral p -wave superconductors has a thermodynamically stable skyrmionic phase between type-I and the usual type-II regimes. This is despite the fact that the model has $U(1) \times \mathbb{Z}_2$ broken symmetry where naive symmetry arguments would rule out skyrmionic excitations. In the skyrmionic phase, the long sought-after half-quantum vortices acquire thermodynamic stability. These objects

can be detected with surface probes through their characteristic profile of magnetic field. The phase transition into a skyrmionic state should be first order, because the energy per flux quantum is decreasing with the skyrmionic topological charge.

The possibly chiral superconductor Sr_2RuO_4 which is frequently described by the model (1) may have a penetration length which is slightly too large to fall into the skyrmionic phase. However in this case, the model predicts metastable skyrmionic excitations (which are slightly more energetic than vortices). Recently sporadic formation of objects with multiple flux quanta were reported in Fig. 2 of Ref. 21. Higher resolution scans of the magnetic field profile could confirm or rule out if the observed objects are skyrmions. Another scenario for flux clustering in this material is type-1.5 superconductivity

which can arise if to take into account its multi-band nature.²²

ACKNOWLEDGMENTS

We thank D. F. Agterberg and J. Carlström for discussions. The work is supported by the Swedish Research Council, and by the Knut and Alice Wallenberg Foundation through the Royal Swedish Academy of Sciences fellowship and by NSF CAREER Award Nos. DMR-0955902. The computations were performed on resources provided by the Swedish National Infrastructure for Computing (SNIC) at National Supercomputer Center at Linköping, Sweden.

-
- ¹ G. E. Volovik, *The Universe in a Helium Droplet* (Oxford University Press, 2009) P. W. Anderson and G. Toulouse, *Phys. Rev. Lett.* **38**, 508 (Feb 1977) E. V. Thuneberg, *ibid.* **56**, 359 (Jan 1986) M. M. Salomaa and G. E. Volovik, *ibid.* **56**, 363 (Jan 1986) *Rev. Mod. Phys.* **59**, 533 (1987) T. A. Tokuyasu, D. W. Hess, and J. A. Sauls, *Phys. Rev. B* **41**, 8891 (May 1990)
 - ² J. Jang, D. G. Ferguson, V. Vakaryuk, R. Budakian, S. B. Chung, P. M. Goldbart, and Y. Maeno, *Science* **331**, 186 (2011)
 - ³ E. Babaev, *Phys. Rev. Lett.* **94**, 137001 (2005)
 - ⁴ S. B. Chung, H. Bluhm, and E.-A. Kim, *Phys. Rev. Lett.* **99**, 197002 (2007)
 - ⁵ S. B. Chung, D. F. Agterberg, and E.-A. Kim, *New Journal of Physics* **11**, 085004 (2009)
 - ⁶ S. B. Chung and S. A. Kivelson, *Phys. Rev. B* **82**, 214512 (2010)
 - ⁷ E. Babaev, J. Jäykkä, and M. Speight, *Phys. Rev. Lett.* **103**, 237002 (2009)
 - ⁸ E. Babaev, *Phys. Rev. Lett.* **89**, 067001 (2002)
 - ⁹ A. Y. Kitaev, *Annals of Physics* **303**, 2 (2003)
 - ¹⁰ A. Knigavko and B. Rosenstein, *Phys. Rev. Lett.* **82**, 1261 (1999) A. Knigavko, B. Rosenstein, and Y. F. Chen, *Phys. Rev. B* **60**, 550 (1999) B. Rosenstein, I. Shapiro, B. Y. Shapiro, and G. Bel, **67**, 224507 (2003) Q. Li, J. Toner, and D. Belitz, **79**, 014517 (2009) *Phys. Rev. Lett.* **98**, 187002 (2007)
 - ¹¹ E. Babaev, *Phys. Rev. Lett.* **88**, 177002 (2002)
 - ¹² L. F. Chibotaru, V. H. Dao, and A. Ceulemans, *Europhys. Lett.* **78**, 47001 (May 2007) L. F. Chibotaru and V. H. Dao, *Phys. Rev. B* **81**, 020502 (Jan 2010) H. Bluhm, N. C. Koshnick, M. E. Huber, and K. A. Moler, *Phys. Rev. Lett.* **97**, 237002 (Dec. 2006) R. Geurts, M. V. Milošević, and F. M. Peeters, *Phys. Rev. B* **81**, 214514 (Jun. 2010) J. C. Piña, C. C. de Souza Silva, and M. V. Milošević, *Phys. Rev. B* **86**, 024512 (Jul. 2012)
 - ¹³ E. Babaev, *Nucl. Phys. B* **686**, 397 (2004) E. Smørgrav, J. Smiseth, E. Babaev, and A. Sudbø, *Phys. Rev. Lett.* **94**, 096401 (2005)
 - ¹⁴ M. A. Silaev, *Phys. Rev. B* **83**, 144519 (2011)
 - ¹⁵ D. F. Agterberg, *Phys. Rev. Lett.* **80**, 5184 (1998)
 - ¹⁶ D. F. Agterberg, *Phys. Rev. B* **58**, 14484 (1998) R. Heeb and D. F. Agterberg, *Phys. Rev. B* **59**, 7076 (1999)
 - ¹⁷ M. Sigrist and D. F. Agterberg, *Prog. Theor. Phys.* **102**, 965 (1999) D. G. Ferguson and P. M. Goldbart, *Phys. Rev. B* **84**, 014523 (2011) V. Vakaryuk, *Phys. Rev. B* **84**, 214524 (Dec 2011)
 - ¹⁸ Y. Matsunaga, M. Ichioka, and K. Machida, *Phys. Rev. Lett.* **92**, 157001 (2004) *Phys. Rev. B* **70**, 100502 (2004) M. Ichioka, Y. Matsunaga, and K. Machida, *Phys. Rev. B* **71**, 172510 (2005)
 - ¹⁹ F. Hecht, O. Pironneau, A. Le Hyaric, and K. Ohtsuka, *The Freefem++ manual* (2007) www.freefem.org
 - ²⁰ E. Babaev, L. D. Faddeev, and A. J. Niemi, *Phys. Rev. B* **65**, 100512 (2002)
 - ²¹ C. W. Hicks, J. R. Kirtley, T. M. Lippman, N. C. Koshnick, M. E. Huber, Y. Maeno, W. M. Yuhasz, M. B. Maple, and K. A. Moler, *Phys. Rev. B* **81**, 214501 (Jun 2010)
 - ²² J. Garaud, D. F. Agterberg, and E. Babaev (Jul. 2012), [arXiv:1207.6395](https://arxiv.org/abs/1207.6395), to appear in *Phys. Rev. B*

Appendix A: Technical details

Functional variation of the free energy (1) with respect to the fields provides Euler-Lagrange equations of motion. In particular, variation with respect to the gauge field defines the total supercurrent

$$\mathbf{J} \equiv \mathbf{J}^{(1)} + \mathbf{J}^{(2)}. \quad (\text{A.1})$$

The contribution of each component there, is given by

$$\begin{aligned} J_x^{(1)} &= \frac{e}{2} \text{Im} [\psi_1^* (D_x \psi_1 + \gamma D_y \psi_2)] \\ J_y^{(1)} &= \frac{e\gamma}{2} \text{Im} [\psi_1^* (D_y \psi_1 + D_x \psi_2)] \\ J_x^{(2)} &= \frac{e\gamma}{2} \text{Im} [\psi_2^* (D_x \psi_2 + D_y \psi_1)] \\ J_y^{(2)} &= \frac{e}{2} \text{Im} [\psi_2^* (D_y \psi_2 + \gamma D_x \psi_1)]. \end{aligned} \quad (\text{A.2})$$

The contributions $|\mathbf{J}^{(1)}|$ and $|\mathbf{J}^{(2)}|$ are displayed for the different solutions. Each contribution to the supercurrent reflects the underlying anisotropies due to the complicated gradient terms (1b).

Simple quantum vortex solutions

In the main part of the text, skyrmionic excitations are discussed. For a comparison, we display in Fig. 6 the solution for a usual integer quantum vortex solution in the model (1). Because of the anisotropies (1b) of the theory, the single quantum vortex is also non-axially symmetric. In contrast to vortices, skyrmions have a non-zero skyrmionic topological charge. Moreover, visual inspection of phase difference $\varphi_2 - \varphi_1$ of the skyrmions provides further arguments of the qualitative difference from vortices. Indeed, for skyrmions, the phase difference $\varphi_2 - \varphi_1$ covers the range $[-\pi/2, \pi/2]$. Thus it links both inequivalent ground states. Phase difference for integer vortex ranges only $[0, \pi/2]$.

ψ_{\pm} parametrization of the condensates

Another parametrization of the condensate is sometimes used in literature. Namely combinations

$$\psi_{\pm} \equiv \frac{\psi_1 \pm \psi_2}{\sqrt{2}} \quad (\text{A.3})$$

are used instead of $\psi_{1,2}$. The free energy functional (1) can be rewritten within this different representation (a special care is there needed in the redefinition of the parameters). Let the total current be

$$\mathbf{J} \equiv \mathbf{J}^{(+)} + \mathbf{J}^{(-)}. \quad (\text{A.4})$$

The contribution of each component in terms of the $\psi_{1,2}$

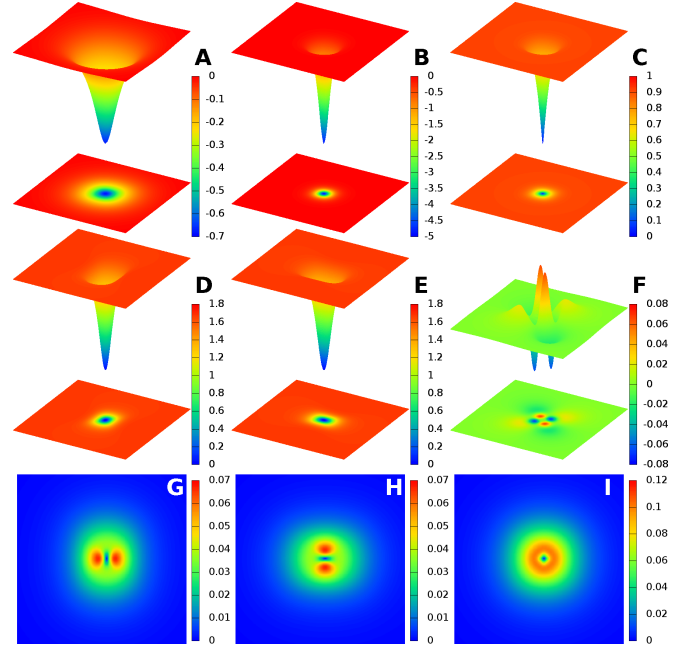


Figure 6. (Color on-line) – A single vortex solution, when $e = 0.2$ and the parameter $\gamma = 0.6$. Displayed quantities are, magnetic flux (A), the (inverted) energy density (B) and the sine of the phase difference $\sin(\varphi_2 - \varphi_1)$ (C). On the second line, the densities of superconducting order parameter components $|\psi_1|^2$ (D), $|\psi_2|^2$ (E), and the ‘doubled phase difference’ $\text{Im}(\psi_1^* \psi_2^2)$ (F). Panels (G) and (resp. H) on the third line, are contribution $|\mathbf{J}^{(1)}|$ (resp. $|\mathbf{J}^{(2)}|$) of ψ_1 (resp. ψ_2) component to supercurrent (A.2). The last panel (I) shows the total supercurrent (A.1). The densities (D and E) and the supercurrents (G and H) of the different components of an integer quantum vortex are very anisotropic. The anisotropies are less perceptible when considering the magnetic field (A) or the energy (B). The main difference with the skyrmions can be seen from panel C. Indeed the phase difference goes from zero at the vortex core to $\pi/2$ faraway, instead of $-\pi/2$ to $\pi/2$ for a skyrmions.

parametrization, is given by

$$\begin{aligned} J_x^{(\pm)} &= \frac{J_x^{(1)} + J_x^{(2)}}{2} \\ &\quad \pm \frac{e}{4} \text{Re} [\psi_1^* \gamma (D_x \psi_2 + D_y \psi_1) - \psi_2^* (D_x \psi_1 + \gamma D_y \psi_2)] \\ J_y^{(\pm)} &= \frac{J_y^{(1)} + J_y^{(2)}}{2} \\ &\quad \pm \frac{e}{4} \text{Re} [\psi_1^* (D_y \psi_2 + \gamma D_x \psi_1) - \psi_2^* \gamma (D_y \psi_1 + D_x \psi_2)], \end{aligned} \quad (\text{A.5})$$

where $\mathbf{J}^{(1)}$ and $\mathbf{J}^{(2)}$ are defined in (A.2).

In order to compare the features of this new parametrization, Fig. 7 show the very same integer flux vortex solution as in Fig. 7, but using the parametrization (A.3). In this new parametrization, the component ψ_+ (panel D) has zero ground state density, while ψ_- (panel E) recovers to non-zero ground state density far

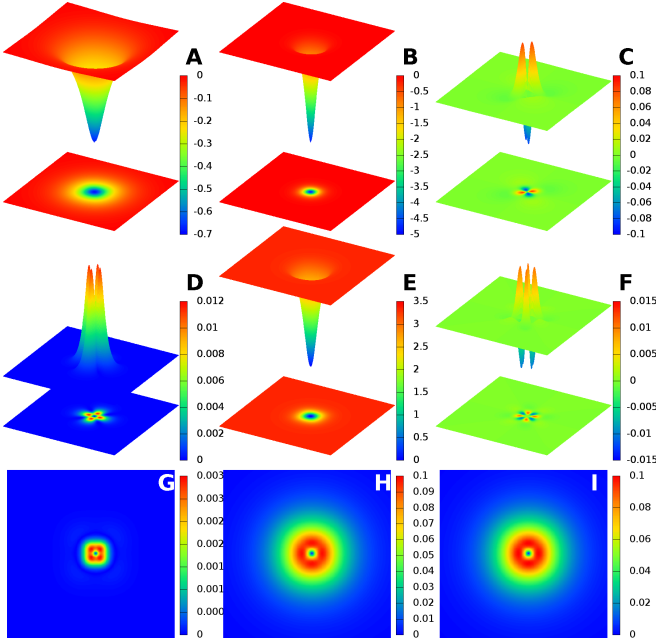


Figure 7. (Color on-line) – A single vortex solution, for the same parameters as in Fig. 6. Quantities displayed now are using the ψ_{\pm} parametrization. Panel (A) is the magnetic flux, and (B) is the (inverted) energy density. The sine of the phase difference $\sin(\varphi_+ - \varphi_-)$ (C). On the second line, the densities of superconducting order parameter components $|\psi_+|^2$ (D), $|\psi_-|^2$ (E), and the ‘doubled phase difference’ $\text{Im}(\psi_+^* \psi_-^2)$ (F). Panels (G) and (resp. H) on the third line, are contribution $|\mathbf{J}^{(-)}|$ (resp. $|\mathbf{J}^{(+)}|$) of ψ_+ (resp. ψ_-) component to supercurrent (A.5). The last panel (I) shows the total supercurrent (A.4).

from the vortex. Both ψ_+ and ψ_- components have a coinciding core singularity. Panel C, showing the sine of the phase difference $\sin(\psi_- - \psi_+)$ exhibit a non-zero winding around the vortex core. This kind of features reproduce the kind of single vortex solution obtained in.¹⁶

The skyrmion solutions are displayed within this field parametrization in Figures 8 and 9. They correspond to solutions provided in the main part.

Appendix B: Numerical Methods – Finite element energy minimization

We provide here details about the numerical methods which are used to construct skyrmions or vortex solutions of the two-components Ginzburg-Landau model (1). The variational problem is defined for numerical computation using a finite element formulation provided by the Freefem++ library.¹⁹ Discretization within finite element formulation is done via a (homogeneous) triangulation over Ω , based on Delaunay-Voronoi algorithm. The domain Ω is chosen here to be a disc whose radius is much larger than the vortex/skyrmion size. In most cases the radius of the disc is 10 to 20 times larger than the size

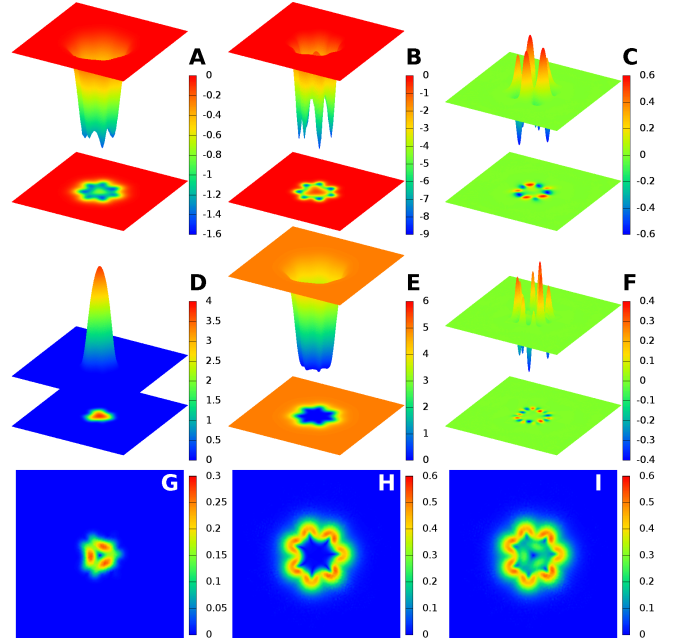


Figure 8. (Color on-line) – The thermodynamically stable skyrmion carrying five flux quanta, presented in Fig. 3 of the manuscript, using the ψ_{\pm} parametrization. Displayed here quantities are the same as in Fig. 7.

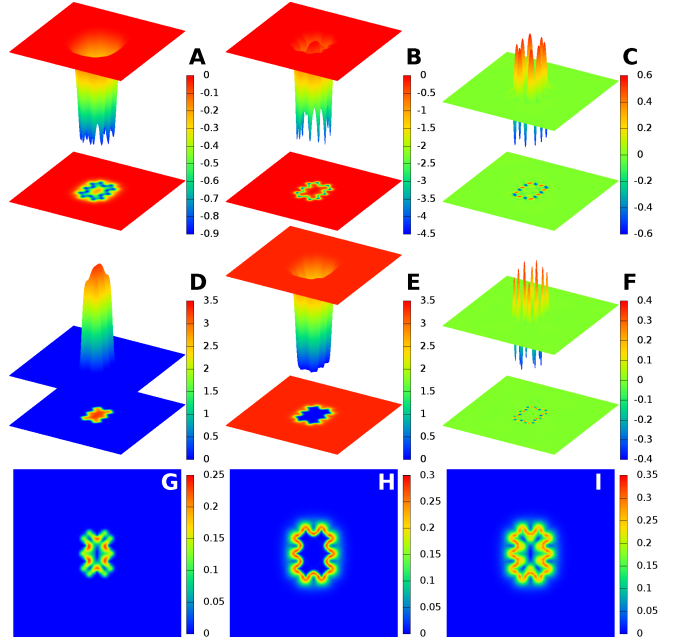


Figure 9. (Color on-line) – The skyrmion carrying eight flux quanta, presented in Fig. 4 of the manuscript, using the ψ_{\pm} parametrization. Displayed here quantities are the same as in Fig. 7.

of a single vortex. This guarantees that all the fields reach their ground state values at the boundary. This ensures that the topological solitons are not affected by the boundary. We performed the additional check that

solutions are not boundary artifacts by computing the energy on the boundary. When the algorithm converges, this quantity is of the order of the numerical accuracy, which indicates that the solutions do not interact with the boundaries of the numerical domain. Functions describing the fields are decomposed on a continuous piecewise quadratic basis over each triangle. The accuracy of such method is controlled through the number of triangles, (we typically used $3 \sim 6 \times 10^4$), the order of expansion of the basis on each triangle (P2 elements being

2nd order polynomial basis on each triangle), and also the order of the quadrature formula for the integral on the triangles.

Once the problem is mathematically well defined, a numerical optimization algorithm is used to solve the variational non-linear problem (*i.e.* to find the minima of \mathcal{F}). Here we used a non-linear conjugate gradient method. The algorithm is iterated until relative variation of the norm of the gradient of the functional \mathcal{F} with respect to all degrees of freedom is less than 10^{-6} .